



# 3D stable and weakly unstable periodic orbits around the Earth near the retrograde co-orbital resonance with the Moon

Kenta Oshima<sup>1</sup>

Received: 31 January 2022 / Accepted: 12 April 2022 / Published online: 27 April 2022  
© The Author(s), under exclusive licence to Springer Nature B.V. 2022

## Abstract

Stable or weakly unstable orbits in cislunar space are attractive as potential locations that natural objects including dust particles may be trapped. Identifying such orbits is not straightforward especially in high-dimensional, many-body dynamical systems. The present paper adopts a strategy of limiting the search space around symmetric periodic orbits in the Earth–Moon spatial circular restricted three-body problem. We find a variety of linearly stable or weakly unstable periodic orbits near the 1 : 1 retrograde resonance with the Moon. Characteristics of the periodic orbits are explored and their stabilities under solar gravitational perturbations are assessed to understand representative behaviours of retrograde co-orbital orbits around the Earth.

**Keywords** Retrograde co-orbital orbit · Periodic orbit · Stability · Orbital flip · Earth–Moon–Sun system

## 1 Introduction

Periodic orbits have been useful for understanding dynamical behaviours of small bodies in space. Stable and unstable manifolds associated with unstable periodic orbits are responsible for transport phenomena or temporary capture (Koon et al. 2011). Weakly unstable periodic orbits can support temporary but sticky capture from afar (Contopoulos and Harsoula 2010). Invariant tori associated with linearly stable periodic orbits offer long-term stability (Lara et al. 2007). These prominent roles of periodic orbits may lead to an efficient search for captured orbits in a high-dimensional phase space by exploring the vicinity of periodic orbits computed in a simplified model (Dei Tos et al. 2018).

The recent discoveries of small bodies moving in long-term stable, retrograde co-orbital orbits around the Sun (Wiegert et al. 2017; Li et al. 2018, 2019) hint the existence of a stability region around the Earth in the 1 : 1 retrograde resonance with the Moon, in addition to the prograde co-orbital stability regions associated with the triangular equilibria (Gómez et al. 2001; Slíz-Balogh et al. 2018, 2019) and lunar quasi-satellite orbits (Minghu et al. 2014; Bezrouk

and Parker 2017; Oshima and Yanao 2019). Although retrograde periodic orbits and associated stable orbits in a variety of resonances have been recently investigated in Sun–planet systems (Morais and Namouni 2013, 2016, 2019; Kotoulas and Voyatzis 2020; Morais et al. 2021; Kotoulas et al. 2022), the unique dynamical environment in the Earth–Moon system with the large Moon-to-Earth mass ratio and the substantial solar gravitational perturbations, which can destabilise orbits in cislunar space (Boudad et al. 2020), would require further investigations. In this context, Oshima (2021) has globally explored stable orbits around the Earth near the 1 : 1 retrograde resonance with the Moon in the Earth–Moon–Sun planar bicircular restricted four-body problem (BCR4BP). The broad stability region for planar orbits has been revealed and relevant periodic orbits have been indicated, but those for inclined orbits are still veiled due to the high dimensionality of the phase space hindering straightforward explorations.

This paper adopts a strategy of limiting the search space around symmetric periodic orbits in the Earth–Moon spatial circular restricted three-body problem (CR3BP) instead of investigating all possible orbits. Since orbits exhibiting finite-time stability, either long-term or temporary, would be characterised by periodic orbits, we focus on initial conditions that symmetric periodic orbits near the 1 : 1 retrograde resonance with the Moon can take. The symmetries of the spatial CR3BP reduce the dimensionality of the search space

✉ K. Oshima  
k.oshima.nt@cc.it-hiroshima.ac.jp

<sup>1</sup> Hiroshima Institute of Technology, 2-1-1 Miyake, Hiroshima, 731-5193, Japan

to three, in which a comprehensive grid search becomes possible. The search reveals three-dimensional stability regions consisting of initial conditions of orbits persistent near the 1 : 1 retrograde resonance with the Moon. Among the stable populations, periodic orbits residing from coplanar to polar states are computed and their characteristics are explored. Finally, we add solar gravitational perturbations on the periodic orbits and investigate their stabilities in the spatial BCR4BP to understand representative behaviours of retrograde co-orbital orbits around the Earth. We find a variety of Sun-perturbed orbits including regular ones exhibiting long-term stability, weakly unstable ones, and substantially destabilised ones. In extreme cases of highly eccentric and highly inclined orbits, orbital flips between prograde and retrograde orbits through the polar inclination are observed and confirmed to be peculiar to the presence of solar gravitational perturbations.

The remainder of the present paper is organised as follows. Section 2 introduces the mathematical models. Section 3 describes the methodology. Section 4 presents the main results. Section 5 summarises concluding remarks.

## 2 Mathematical models

This section introduces the spatial versions of the Earth–Moon CR3BP and Earth–Moon–Sun BCR4BP used in the present work. These models are concerned with the motion of a massless particle under the gravitational influences of the massive bodies. We assume that the Earth and Moon revolve in circular orbits around their barycentre and the Sun and the Earth–Moon barycentre revolve in circular orbits around their common barycentre on the same orbital plane of the Earth and Moon. The motion of a particle is not limited on the orbital plane of the massive bodies.

### 2.1 Equations of motion

In both models, we adopt the Earth–Moon rotating frame to represent the non-dimensional equations of motion

$$\begin{aligned} \ddot{x} - 2\dot{y} &= -\frac{\partial \bar{U}}{\partial x}, \\ \ddot{y} + 2\dot{x} &= -\frac{\partial \bar{U}}{\partial y}, \\ \ddot{z} &= -\frac{\partial \bar{U}}{\partial z}, \end{aligned} \tag{1}$$

with the effective potential in the CR3BP (Szebehely 1967)

$$\bar{U} = \bar{U}_{3BP} := -\frac{1}{2}(x^2 + y^2) - \frac{1-\mu}{r_1} - \frac{\mu}{r_2} - \frac{1}{2}\mu(1-\mu), \tag{2}$$

and that in the BCR4BP (Simó et al. 1995)

$$\bar{U} = \bar{U}_{4BP} := \bar{U}_{3BP} - \frac{m_S}{r_3} + \frac{m_S}{\rho^2}(x \cos \theta_S + y \sin \theta_S), \tag{3}$$

where

$$\begin{aligned} r_1 &:= \sqrt{(x + \mu)^2 + y^2 + z^2}, \\ r_2 &:= \sqrt{(x - 1 + \mu)^2 + y^2 + z^2}, \\ r_3 &:= \sqrt{(x - \rho \cos \theta_S)^2 + (y - \rho \sin \theta_S)^2 + z^2}, \\ \theta_S &:= \theta_{S0} + \omega_S t, \end{aligned} \tag{4}$$

and  $\theta_{S0}$  is the initial solar phase angle at time  $t = 0$ . See Topputo (2013) for the physical constants used in this paper. We also use  $v_x$ ,  $v_y$ , and  $v_z$  to represent the velocity components  $\dot{x}$ ,  $\dot{y}$ , and  $\dot{z}$ , respectively.

When  $m_S = 0$ , i.e., ignoring the mass of the Sun, the BCR4BP is reduced to the Earth–Moon CR3BP and the Jacobi energy

$$C := -(\dot{x}^2 + \dot{y}^2 + \dot{z}^2) - 2\bar{U}_{3BP} \tag{6}$$

is a constant of motion.

### 2.2 Symmetries in the CR3BP

The equations of motion in the spatial CR3BP are invariant under the following transformations (Russell 2006):

$$s_1 : (x, y, z, v_x, v_y, v_z, t) \rightarrow (x, -y, -z, -v_x, v_y, v_z, -t), \tag{7}$$

$$s_2 : (x, y, z, v_x, v_y, v_z, t) \rightarrow (x, -y, z, -v_x, v_y, -v_z, -t), \tag{8}$$

$$s_3 : (x, y, z, v_x, v_y, v_z, t) \rightarrow (x, y, -z, v_x, v_y, -v_z, t). \tag{9}$$

$s_1$ ,  $s_2$ , and  $s_3$  correspond to the symmetries with respect to the  $x$ -axis,  $xz$ -plane, and  $xy$ -plane, respectively. Consider a trajectory propagated forward in time from a certain initial condition. The symmetries  $s_1$  and  $s_2$  indicate the existence of time-reversal, mirror-image solutions with respect to the  $x$ -axis and  $xz$ -plane, respectively, whereas  $s_3$  gives a mirror-image solution with respect to the  $xy$ -plane with no reversal of time.

## 3 Methodology

### 3.1 Grid search

The original dimensionality of the phase space in the spatial CR3BP is six (position and velocity) indicating that a comprehensive search is computationally difficult. Instead, our

**Table 1** Search conditions in non-dimensional units with  $y_0 = v_{x0} = z_0 = 0$  (axi-symmetric case)

Parameter	Minimum	Maximum	Number of grids
$x_0$	-3	3	300
$v_{z0}$	0	10	300
$C_0$	-3	3	300

strategy limits the search space to possible initial conditions of symmetric periodic orbits around the Earth in the vicinity of the 1 : 1 retrograde resonance with the Moon.

In the similar way as defined in Oshima (2021), stability regions in this paper consist of initial conditions of trajectories persistent for longer than one year in the vicinity of the 1 : 1 retrograde resonance with the Moon, i.e.,  $-0.6 < K < -0.4$  and  $h_z < 0$ , where the Kepler energy around the Earth

$$K := \frac{(v_x - y)^2 + (v_y + x + \mu)^2 + v_z^2}{2} - \frac{1 - \mu}{r_1} \quad (10)$$

and the out-of-plane component of the angular momentum around the Earth

$$h_z := (x + \mu)(v_y + x + \mu) - y(v_x - y). \quad (11)$$

Since  $K$  and  $h_z$  are quantities in the two-body problem with respect to the Earth, they can temporarily be disturbed via close encounters with the Moon. Therefore, we evaluate  $K$  and  $h_z$  only when a trajectory is far from the Moon satisfying  $r_2 > 0.5$ .

The symmetry  $s_1$  in Eq. (7) implies that periodic orbits symmetric with respect to the  $x$ -axis may start from  $y_0 = v_{x0} = z_0 = 0$ . Similarly, the symmetry  $s_2$  in Eq. (8) may lead to initial conditions  $y_0 = v_{x0} = v_{z0} = 0$  for those symmetric with respect to the  $xz$ -plane. In both cases, the remaining dimensionality of the search space is three. Furthermore, the symmetry  $s_3$  in Eq. (9) reduces the search space for the out-of-plane components by half.

Tables 1 and 2 summarise the search conditions. Note that the initial Jacobi energy  $C_0$  is adopted instead of  $v_{y0}$ , which is calculated by

$$v_{y0} = \pm \sqrt{-v_{x0}^2 - v_{z0}^2 - C_0 - 2\bar{U}_{3BP}(x_0, y_0, z_0)}. \quad (12)$$

The search conditions in Tables 1 and 2 can generate initial conditions with  $r_2 < 0.5$ . In that case, we propagate them regardless of their  $K$  and  $h_z$ . If  $r_2 > 0.5$  is initially satisfied, we only propagate those satisfying  $-0.6 < K < -0.4$  and  $h_z < 0$ . We stop propagations if one of the following conditions is satisfied: propagation time exceeds one year; a trajectory violates  $-0.6 < K < -0.4$  or  $h_z < 0$  when  $r_2 > 0.5$ ; a trajectory collides with the surface of the Earth or Moon. There exist trajectories that initially satisfy  $r_2 < 0.5$

**Table 2** Search conditions in non-dimensional units with  $y_0 = v_{x0} = v_{z0} = 0$  ( $xz$ -planar symmetric case)

Parameter	Minimum	Maximum	Number of grids
$x_0$	-3	3	300
$z_0$	0	3	300
$C_0$	-3	3	300

and never escape from the vicinity of the Moon, which are excluded from the current scope.

### 3.2 Initial guesses for periodic orbits

Linearly stable or weakly unstable periodic orbits that support the existence of stable orbits should be embedded in the stability regions found in the grid search. Among the stable orbits, we extract initial guesses for the periodic orbits satisfying

$$\sqrt{(x - x_0)^2 + (z - z_0)^2 + (v_x - v_{x0})^2 + (v_y - v_{y0})^2 + (v_z - v_{z0})^2} < 0.1 \quad (13)$$

on the surface of section  $y = 0$  ( $y_0$  is always zero) for the first time within 35 days.

Although a larger tolerance in terms of the difference in position and velocity would be useful for finding highly unstable orbits, we adopt the tolerance because the periodic orbits of interest are linearly stable or weakly unstable ones. Additionally, the tolerance in terms of a period results in a web of periodic orbits rich enough as will be shown later and thus longer-period orbits are out of the scope of the present paper.

### 3.3 Differential correction

Once a suitable initial guess for a periodic orbit is found, a differential correction scheme (Russell 2006) is applied to iteratively make it converge into a periodic orbit. The scheme exploits a state transition matrix (STM)  $\Phi(t_1, t_0)$  mapping the initial deviation from initial time  $t_0$  to final time  $t_1$ . The STM is computed by propagating

$$\dot{\Phi}(t, t_0) = A(t)\Phi(t, t_0), \quad \Phi(t_0, t_0) = I_6, \quad (14)$$

with the equations of motion in the CR3BP from  $t_0$  to  $t_1$ , where  $A(t)$  is the Jacobian matrix of the system and  $I_6$  is the  $6 \times 6$  identity matrix. We use the notation  $\Phi_{ij}$  to represent an element in the  $i$ th row and  $j$ th column of the STM.

The time-reversal symmetries  $s_1$  and  $s_2$  in Eqs. (7) and (8) suggest that a periodic orbit of the corresponding symmetry with  $y_0 = v_{x0} = z_0 = 0$  (axi-symmetric case) and  $y_0 = v_{x0} = v_{z0} = 0$  ( $xz$ -planar symmetric case), respectively, must satisfy  $y_1 = v_{x1} = z_1 = 0$  and  $y_1 = v_{x1} =$

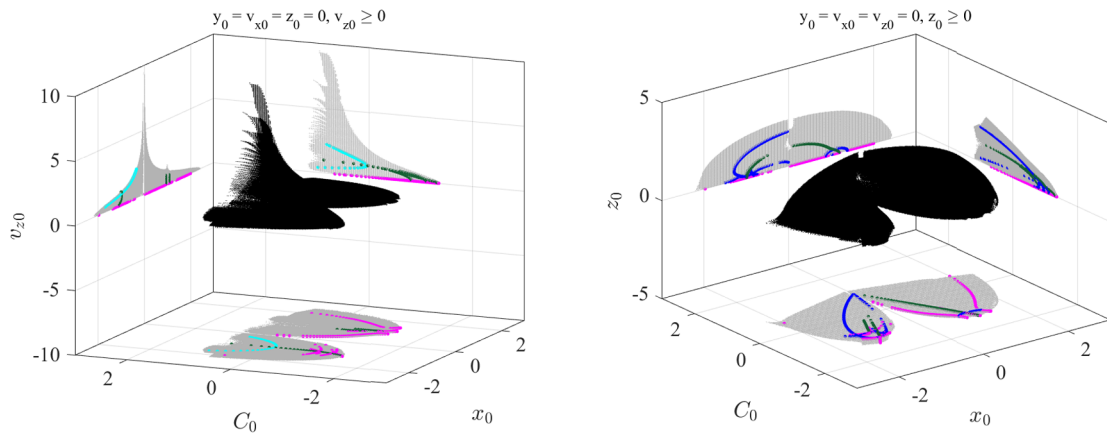


**Fig. 1** Initial conditions of stable orbits (black) persistent for longer than one year in the vicinity of the 1 : 1 retrograde resonance with the Moon found via the grid search with  $y_0 = v_{x0} = z_0 = 0$  (left panel) and  $y_0 = v_{x0} = v_{z0} = 0$  (right panel), respectively. On each plane, initial

conditions of the stable orbits (grey) as well as those of periodic orbits classified into planar (magenta), axi-symmetric (cyan),  $xz$ -planar symmetric (blue), and doubly symmetric (green) ones are projected

$v_{z1} = 0$ , respectively, after a half period. In the similar manner, a planar symmetric periodic orbit with an initial condition  $y_0 = v_{x0} = 0$  must satisfy  $y_1 = v_{x1} = 0$  after a half period.

The differential correction scheme for three-dimensional periodic orbits may be derived as

$$\begin{aligned} x_0 &\rightarrow x_0 - \delta x_0, \\ v_{y0} &\rightarrow v_{y0} - \delta v_{y0}, \end{aligned} \tag{15}$$

where the correction terms for axi-symmetric orbits are

$$\begin{bmatrix} \delta x_0 \\ \delta v_{y0} \end{bmatrix} = \left[ \begin{bmatrix} \Phi_{31} & \Phi_{35} \\ \Phi_{41} & \Phi_{45} \end{bmatrix} - \frac{1}{v_{y1}} \begin{bmatrix} v_{z1} \\ v_{x1} \end{bmatrix} \begin{bmatrix} \Phi_{21} & \Phi_{25} \end{bmatrix} \right]^{-1} \begin{bmatrix} z_1 \\ v_{x1} \end{bmatrix} \tag{16}$$

and those for  $xz$ -planar symmetric orbits are

$$\begin{bmatrix} \delta x_0 \\ \delta v_{y0} \end{bmatrix} = \left[ \begin{bmatrix} \Phi_{41} & \Phi_{45} \\ \Phi_{61} & \Phi_{65} \end{bmatrix} - \frac{1}{v_{y1}} \begin{bmatrix} v_{x1} \\ v_{z1} \end{bmatrix} \begin{bmatrix} \Phi_{21} & \Phi_{25} \end{bmatrix} \right]^{-1} \begin{bmatrix} v_{x1} \\ v_{z1} \end{bmatrix}. \tag{17}$$

There are special three-dimensional orbits converged by the scheme in Eq. (16) or Eq. (17) that satisfy both  $y = v_x = z = 0$  and  $y = v_x = v_z = 0$  along the revolution. Such orbits enjoying both of the symmetries are doubly symmetric orbits (Russell 2006) and they are distinguished from axi-symmetric or  $xz$ -planar symmetric orbits after convergence.

The scheme for planar periodic orbits may be derived as

$$v_{y0} \rightarrow v_{y0} - \delta v_{y0}, \tag{18}$$

where

$$\delta v_{y0} = \frac{v_{x1}}{\Phi_{45} - \frac{v_{x1}}{v_{y1}} \Phi_{25}}. \tag{19}$$

## 4 Result

### 4.1 Characteristics of periodic orbits

Figure 1 presents initial conditions of stable orbits (black) persistent for longer than one year in the vicinity of the 1 : 1 retrograde resonance with the Moon found via the grid search with  $y_0 = v_{x0} = z_0 = 0$  (left panel) and  $y_0 = v_{x0} = v_{z0} = 0$  (right panel), respectively, in the corresponding three-dimensional search space. On each plane of the search space, initial conditions of the stable orbits (grey) as well as those of periodic orbits are projected for clear visualisation. The periodic orbits are classified into planar (magenta), axi-symmetric (cyan),  $xz$ -planar symmetric (blue), and doubly symmetric (green) orbits. Note that, according to the symmetry  $s_3$  in Eq. (9), flipping the sign of the out-of-plane components of the initial conditions doubles the number of the three-dimensional stable orbits in a straightforward manner. The search ranges in Tables 1 and 2 sufficiently encompass the initial conditions of the stable orbits, which possess two main stability regions, respectively, separated by the dynamically sensitive region around the Earth at  $x \approx -\mu$ . The initial conditions of the periodic orbits are widely distributed among those of the stable orbits, nevertheless not in a comprehensive manner possibly due to the tolerance in terms of a period introduced in Sect. 3.2.

Although some structures of families of periodic orbits are visible in Fig. 1, it is more intuitive to classify them based on geocentric orbital elements. Since Fig. 1 includes initial conditions that are in the vicinity of the Moon, we investigate intersections of the periodic orbits with the surface of section  $y = 0$  and  $v_y > 0$ , on which  $x$  is confirmed to be always negative.

Figure 2 visualises distributions of geocentric orbital elements (semi-major axis  $a$ , eccentricity  $e$ , and inclination  $i$ )

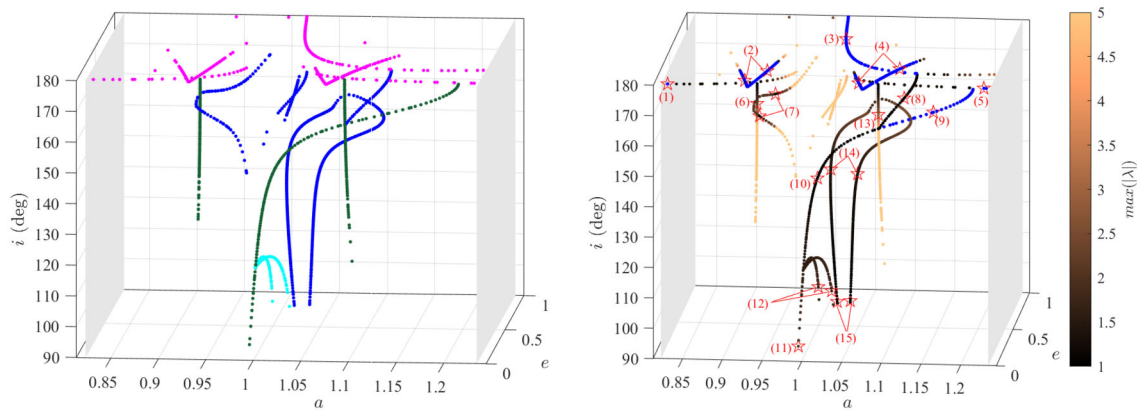


**Fig. 2** Distributions of geocentric orbital elements of the periodic orbits on the surface of section  $y = 0$  and  $v_y > 0$ . The orbits of interest are bounded by  $i > 90^\circ$  and  $-0.6 < K < -0.4$  corresponding to the grey surfaces with constant  $a$ . (Left panel) The colour classifies the or-

bits into planar (magenta), axi-symmetric (cyan),  $xz$ -planar symmetric (blue), and doubly symmetric (green) ones. (Right panel) The colour denotes the maximum absolute value among six eigenvalues of the monodromy matrix. Linearly stable periodic orbits are shown in blue

**Table 3** The initial conditions ( $y_0 = v_{x0} = 0$ ) and the period ( $T$ ) of the sample periodic orbits indicated in Fig. 2(right)

Sample number	$x_0$	$z_0$	$v_{y0}$	$v_{z0}$	$T$
(1)	0.812709030	0	-1.94490125	0	2.75149510
(2)	-1.17391304	0	1.97270464	0	6.26067341
(3)	0.311036789	0	-2.59118566	0	6.34524340
(4)	-1.17391304	0	2.04255911	0	6.24997582
(5)	-1.17391304	0	2.10807126	0	3.51465476
(6)	0.921317268	0	-2.03329970	0.133333333	6.29988560
(7)	-1.15754856	0.140000000	1.97093249	0	6.39841842
(8)	0.880822285	0.110000000	-2.06341968	0	6.77545909
(9)	-1.12738404	0	2.06657997	0.133333333	6.84238502
(10)	-1.01262286	0	1.86969545	0.500000000	6.33176043
(11)	-1.00027085	0	1.07364225	1.000000000	6.25629646
(12)	-1.67549069	0	1.72704292	0.433333333	6.26454251
(13)	-0.980681162	0.180000000	2.01793883	0	6.29732696
(14)	-1.19786182	0.930000000	1.76762026	0	6.37370218
(15)	-0.0173056267	0.220000000	2.83649588	0	6.33644612

on the surface of section. The left panel classifies the symmetry property and the right panel highlights the linear stability of the periodic orbits. The colour in the left panel classifies the orbits into planar (magenta), axi-symmetric (cyan),  $xz$ -planar symmetric (blue), and doubly symmetric (green) ones. Axi-symmetric orbits rarely appear in the conditions investigated in the present paper. The linear stability is assessed based on eigenvalues of the monodromy matrix  $\Phi(T, 0)$  (STM over a full period  $T$ ). The colour in the right panel denotes the maximum absolute value among six eigenvalues of the monodromy matrix,  $\max(|\lambda|)$ , indicating the strength of instability (Koon et al. 2011). Linearly stable periodic orbits (blue) having unity  $\max(|\lambda|)$  only exist in the low-inclination regime ( $i > 165^\circ$ ), but some highly

inclined, weakly unstable orbits exist including polar ones ( $i \approx 90^\circ$ ). The orbits of interest are bounded by  $i > 90^\circ$  and  $-0.6 < K < -0.4$  corresponding to the grey surfaces with constant  $a$  and those outside the boundaries are out of the scope of the present paper.

Sample solutions are marked with stars in the right panel and corresponding orbits will be presented in the next section. The samples (1)–(5) are linearly stable, planar orbits and the samples (6)–(15) are three-dimensional ones. Among the three-dimensional orbits, only the sample (9) is linearly stable. The other three-dimensional orbits are weakly unstable. Note that a doubly revolutionary geometry in the Earth–Moon rotating frame may produce two different sets of the orbital elements on the surface of section over

**Fig. 3** The sample (1) propagated in the CR3BP (red) and BCR4BP (grey)

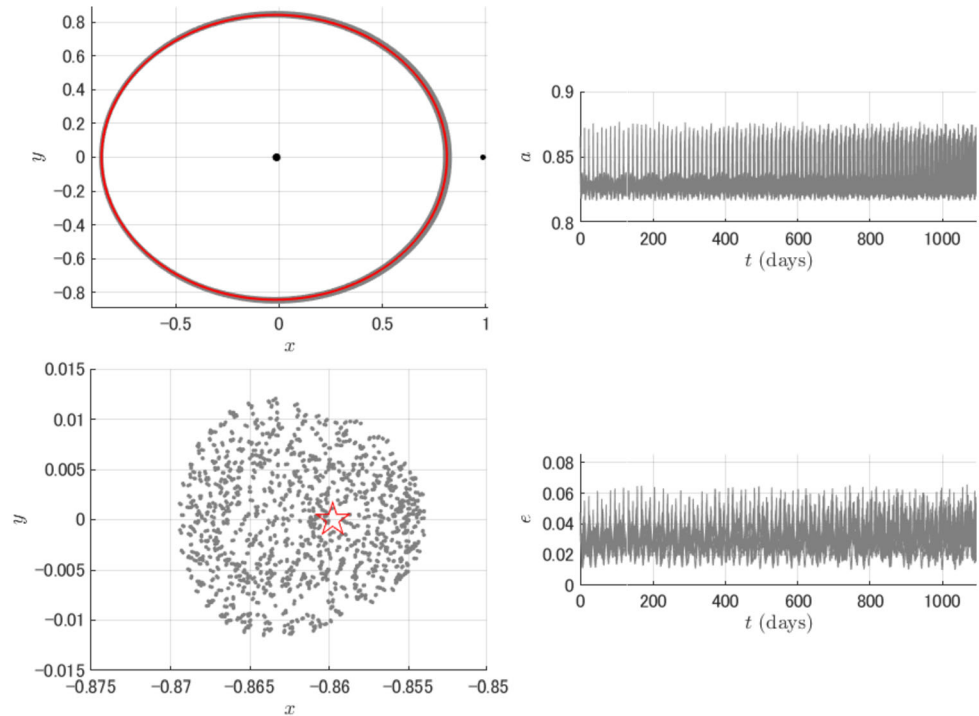
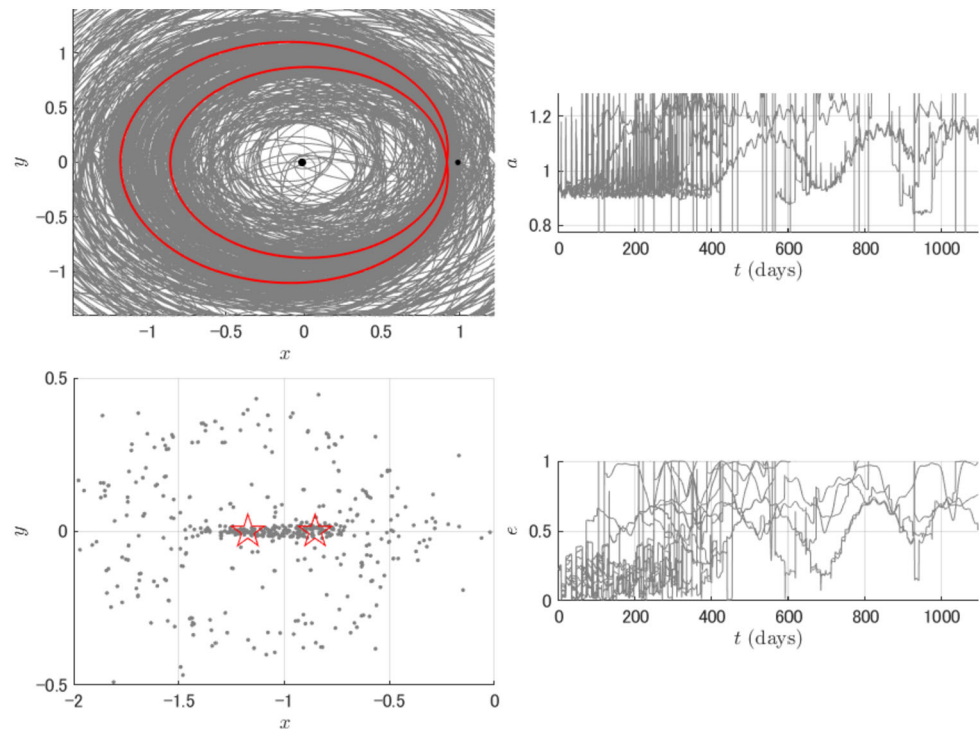


**Fig. 4** The sample (2) propagated in the CR3BP (red) and BCR4BP (grey)



one period, such as the samples (2), (4), (7), (12), (14), and (15). Table 3 summarises the initial conditions and the period of the sample periodic orbits.

Planar periodic orbits near the 1 : 1 retrograde resonance with the Moon or Jupiter have been well studied (Broucke 1968; Morais and Namouni 2013; Oshima 2021), but only a few studies have addressed three-dimensional or-

bits (Morais and Namouni 2016, 2019). A variety of three-dimensional periodic orbits near the 1 : 1 retrograde resonance with the Jupiter directly bifurcated from the planar orbits has been identified in Morais and Namouni (2019) and we could not find qualitatively different properties from those in Fig. 2(right) computed with the Moon-to-Earth mass ratio. We point out that families of three-dimensional

**Fig. 5** The sample (3) propagated in the CR3BP (red) and BCR4BP (grey)

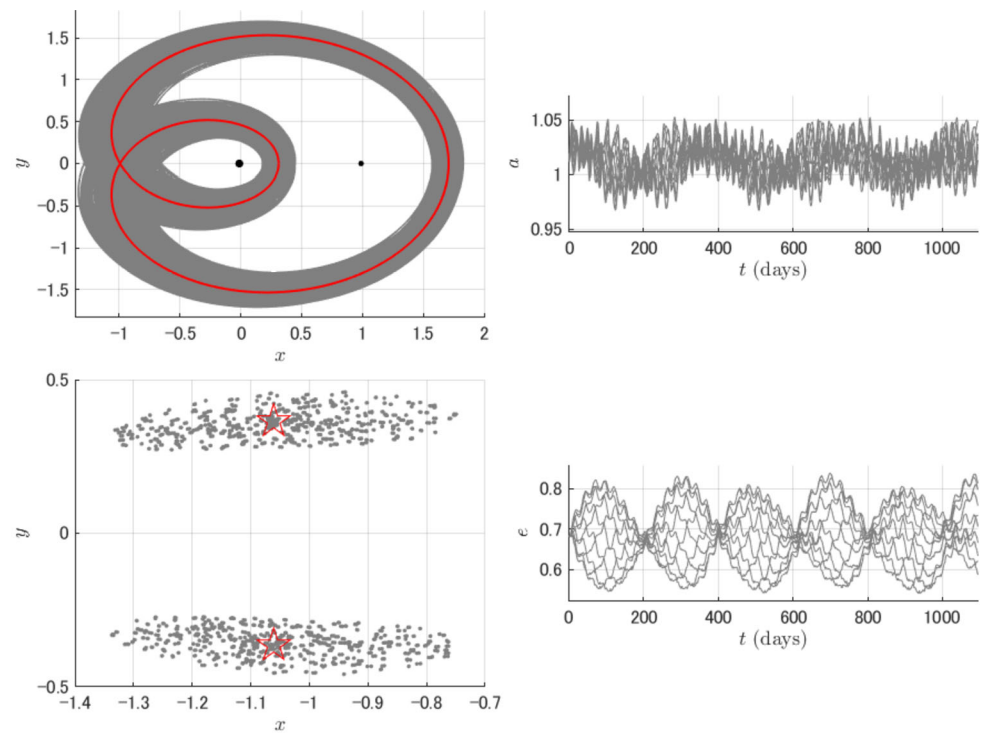
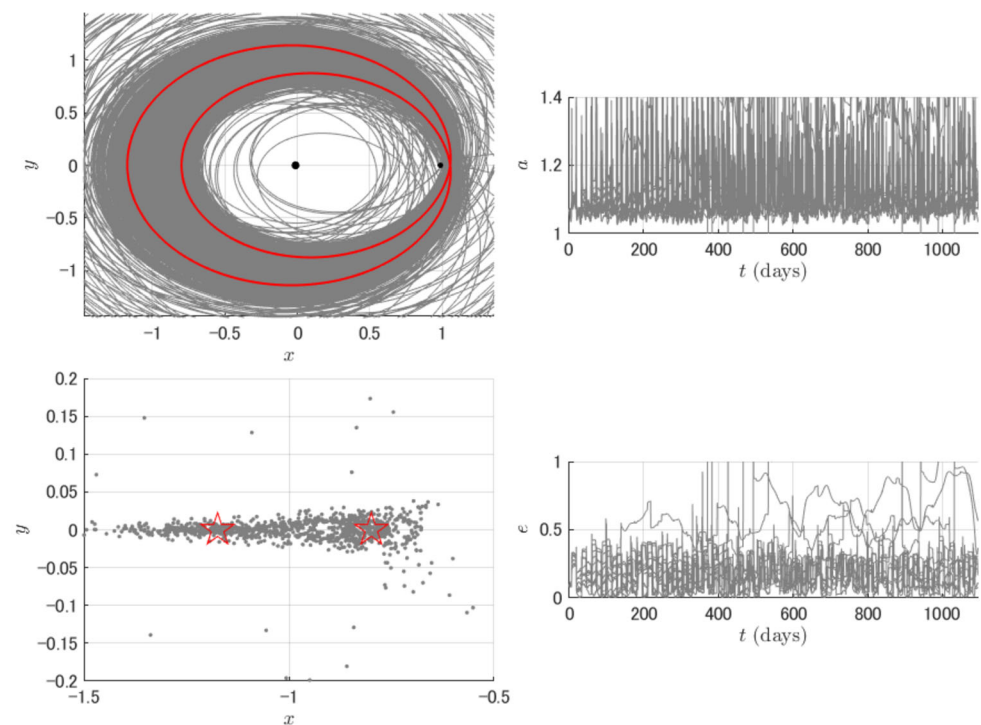


**Fig. 6** The sample (4) propagated in the CR3BP (red) and BCR4BP (grey)



orbits further bifurcated from three-dimensional ones, such as those including the samples (12), (14), and (15), have not been reported in Morais and Namouni (2019). We also could not find earlier works mentioning the families of three-dimensional orbits including the samples (6) and (7).

## 4.2 Sample orbits

This section assesses the impact of solar gravitational perturbations onto the stability of the retrograde periodic orbits. The sample periodic orbits are propagated not only in the Earth–Moon CR3BP but also in the Earth–Moon–Sun

**Fig. 7** The sample (5) propagated in the CR3BP (red) and BCR4BP (grey)

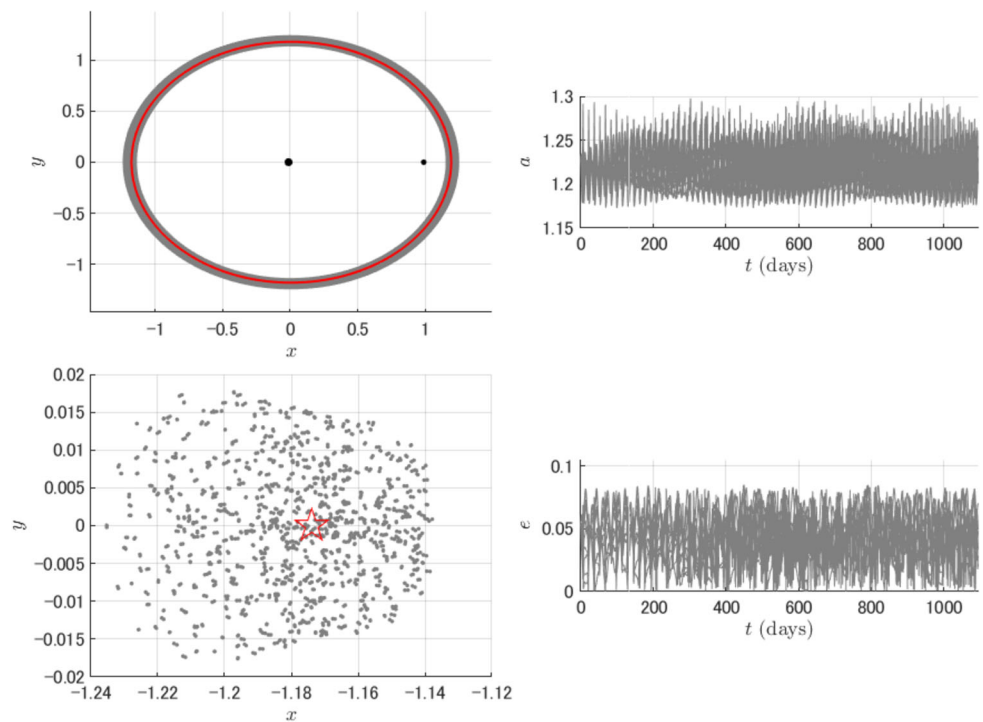
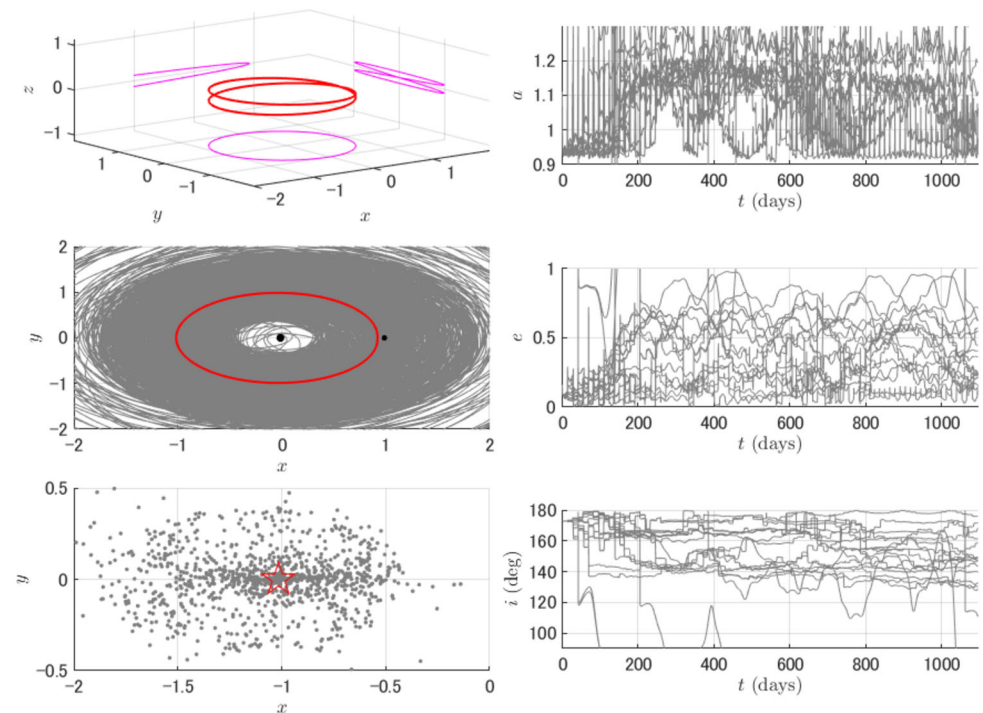


**Fig. 8** The sample (6) propagated in the CR3BP (red) and BCR4BP (grey)



BCR4BP for three years under solar gravitational perturbations with 20 clones of various initial solar phase angles equally distributed in the range of  $0 \leq \theta_{S0} < 2\pi$ . The left panels in Figs. 3–17 present the sample orbits in the Earth–Moon rotating frame computed in the CR3BP (red) and those propagated in the BCR4BP (grey) and the cor-

responding intersections with the surface of section  $v_x = 0$  and  $v_y > 0$  around the periodic orbits (star). The right panels show time evolutions of the geocentric orbital elements in the BCR4BP. Geometries of periodic orbits in the  $xyz$ -space and time evolutions of the inclination of the planar orbits are omitted in Figs. 3–7.



**Fig. 9** The sample (7) propagated in the CR3BP (red) and BCR4BP (grey)

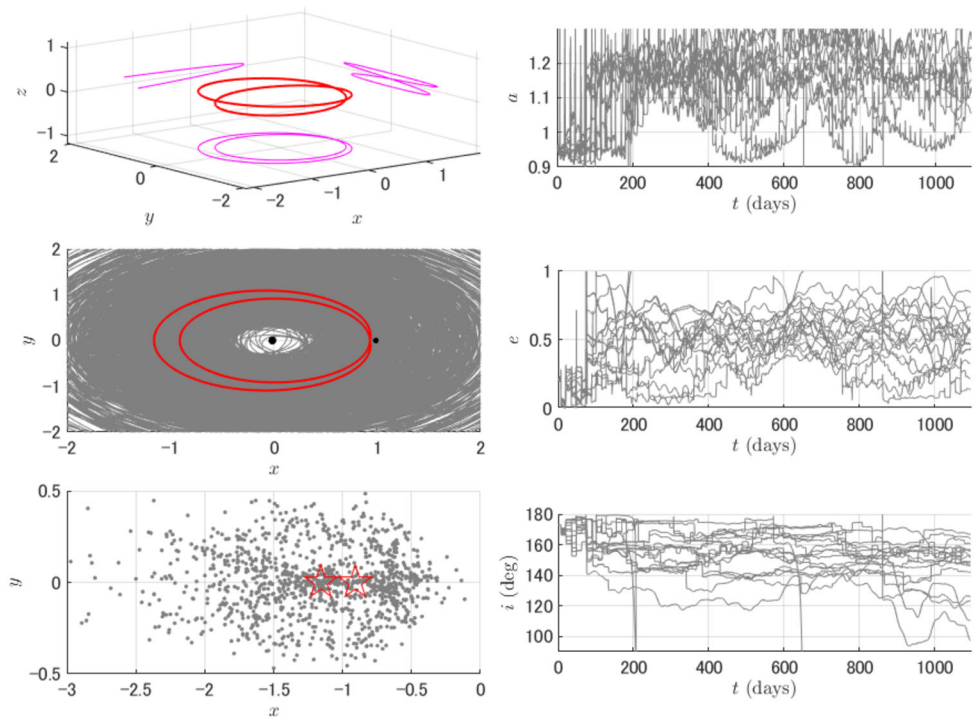
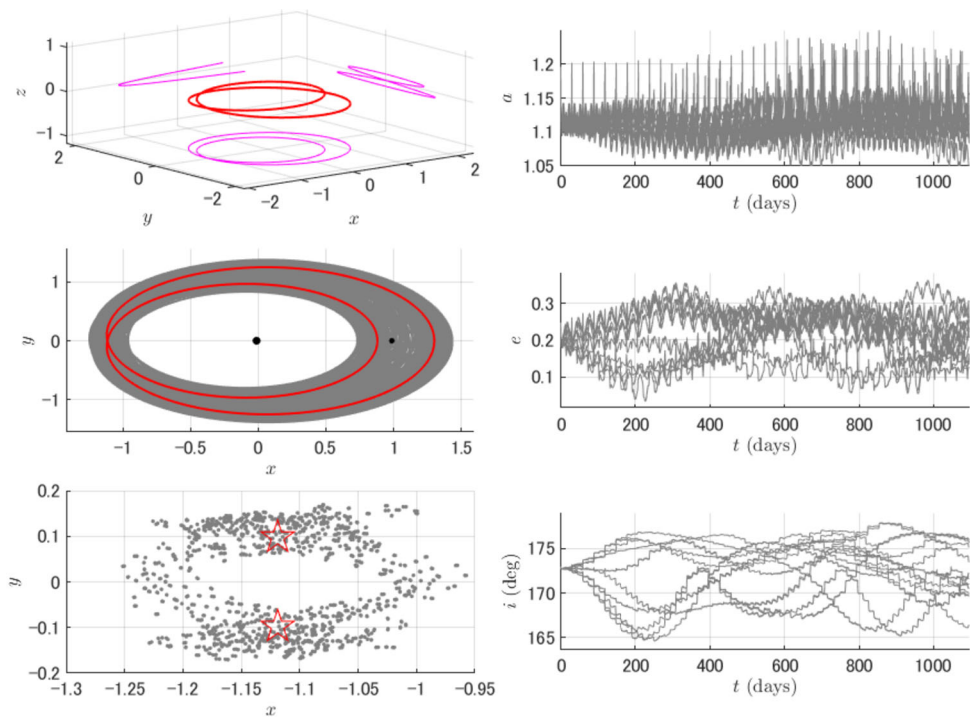


**Fig. 10** The sample (8) propagated in the CR3BP (red) and BCR4BP (grey)



The originally stable orbits of the samples (1), (3), (5), and (9) exhibit remarkable stability even under solar gravitational perturbations, and thus their orbital neighbourhoods could be potentially interesting locations that natural objects such as dust particles may be trapped. On the other hand, the Sun-perturbed trajectories of the originally stable, planar orbits of the samples (2) and (4) are substantially desta-

bilised possibly due to the low perilune altitudes. Many of the orbital clones of the three-dimensional orbits of the samples (6) and (7) shortly escape from the vicinity of the original states.

It is interesting to note that the weakly unstable orbits of the samples (8), (10), (11), (13), and (14) are fairly robust against solar gravitational perturbations. Their instabil-

**Fig. 11** The sample (9) propagated in the CR3BP (red) and BCR4BP (grey)

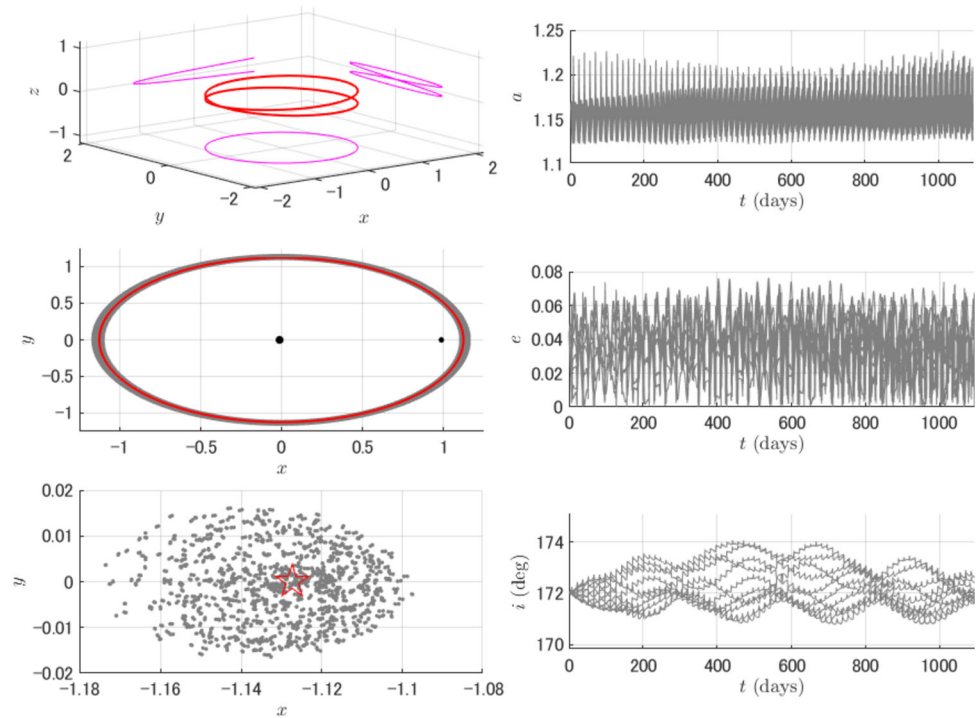
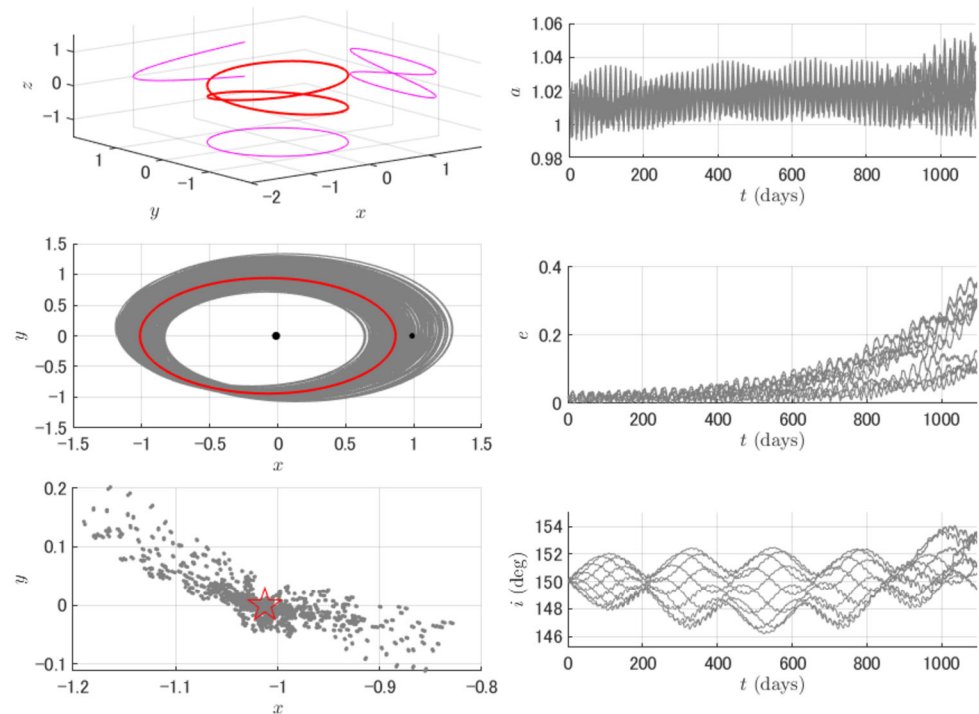


**Fig. 12** The sample (10) propagated in the CR3BP (red) and BCR4BP (grey)



ity would limit the performance of trapping objects, but the weakly unstable nature may produce sticky captures from distant places. The mildly inclined orbits of the samples (10) and (14) as well as the highly inclined ones of the sample (11) indicate the significance of exploring the three-dimensional space.

The remaining samples (12) and (15) are highly eccentric, highly inclined orbits. Their Sun-perturbed trajectories reach  $e \approx 1$  and experience orbital flips between prograde and retrograde orbits through  $i = 90^\circ$ . Especially, those of the sample (15) collectively show the extreme behaviour asymptotic to the polar inclination and always stay in the

**Fig. 13** The sample (11) propagated in the CR3BP (red) and BCR4BP (grey)

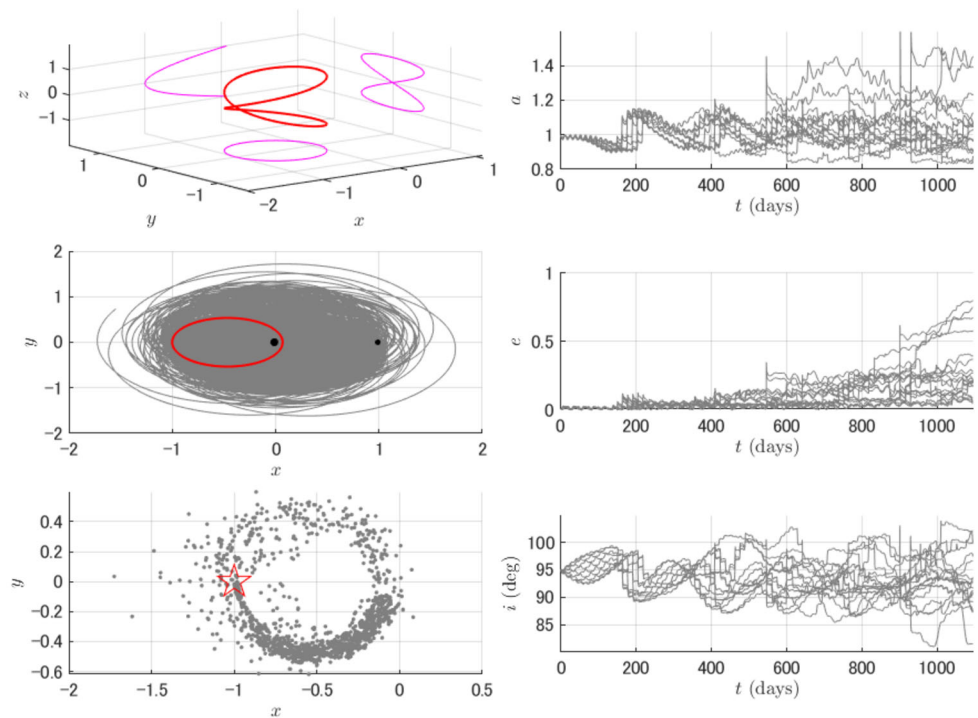
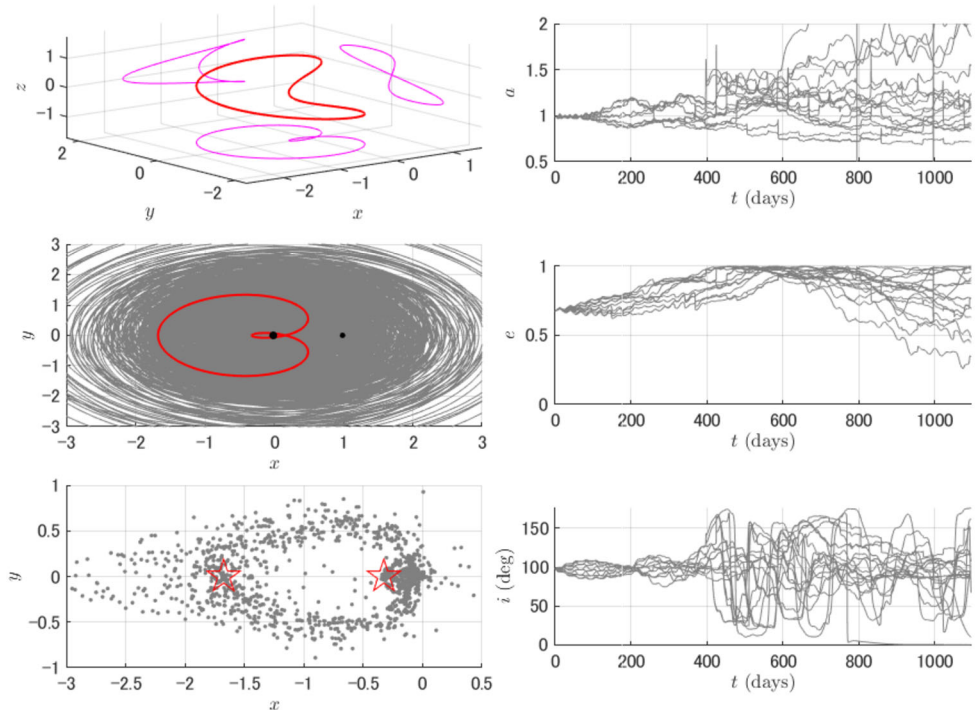


**Fig. 14** The sample (12) propagated in the CR3BP (red) and BCR4BP (grey)



vicinity of the co-orbital resonance. Indeed, many of the orbital clones of the sample (12) and all clones of the sample (15) collide with the surface of the Earth when  $e \approx 1$  meaning the existence of natural Sun-perturbed pathways between the Earth and the near-polar periodic orbits.

### 4.3 Impact of solar gravity on orbital flips

To highlight the significance of solar gravitational perturbations inducing the orbital flips, we investigate long-term behaviours of unstable manifolds associated with the weak instability of the periodic orbit of the sample (15) in the

**Fig. 15** The sample (13) propagated in the CR3BP (red) and BCR4BP (grey)

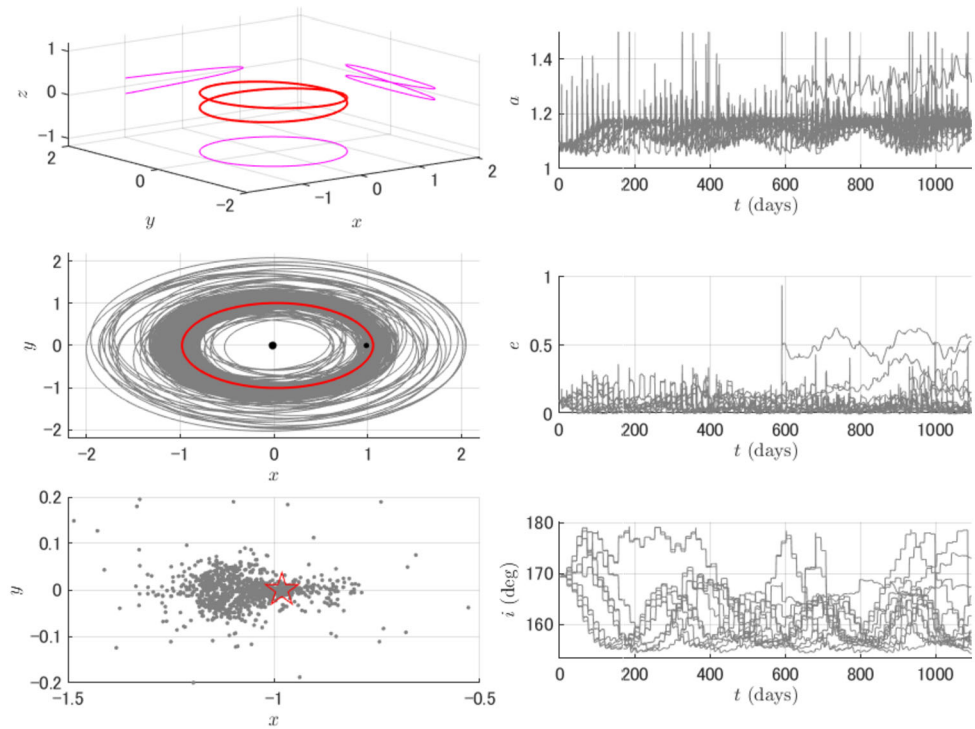
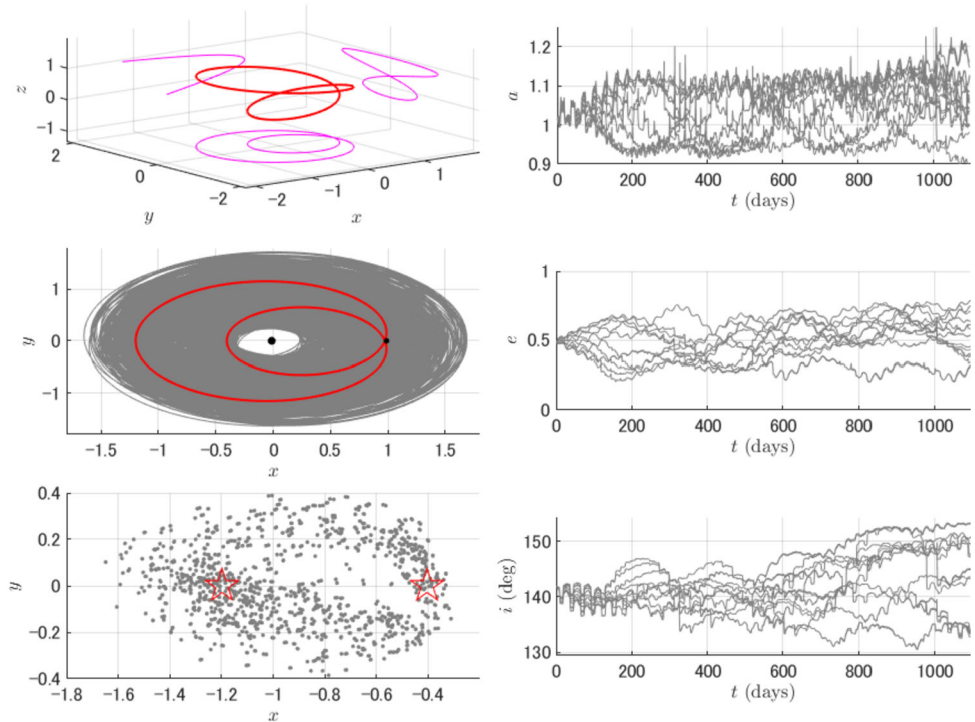


**Fig. 16** The sample (14) propagated in the CR3BP (red) and BCR4BP (grey)



Earth–Moon CR3BP. The unstable manifolds are computed by propagating perturbed states (Koon et al. 2011)

$$X_U(\tau) := X(\tau) \pm \epsilon v_U(\tau), \tag{20}$$

where  $\tau$  is a time-like parameter representing a phase on the periodic orbit,  $X$  is a state vector,  $v_U$  is an eigenvector as-

sociated with an unstable eigenvalue  $\lambda > 1$ , and  $\epsilon = 10^{-5}$  is the magnitude of the perturbation in non-dimensional units. There is only one unstable eigenvalue for the periodic orbit. We globalise the unstable manifolds from 20 phases equally distributed in the range of  $0 \leq \tau < T$  on the orbit of a period  $T$ .

**Fig. 17** The sample (15) propagated in the CR3BP (red) and BCR4BP (grey)

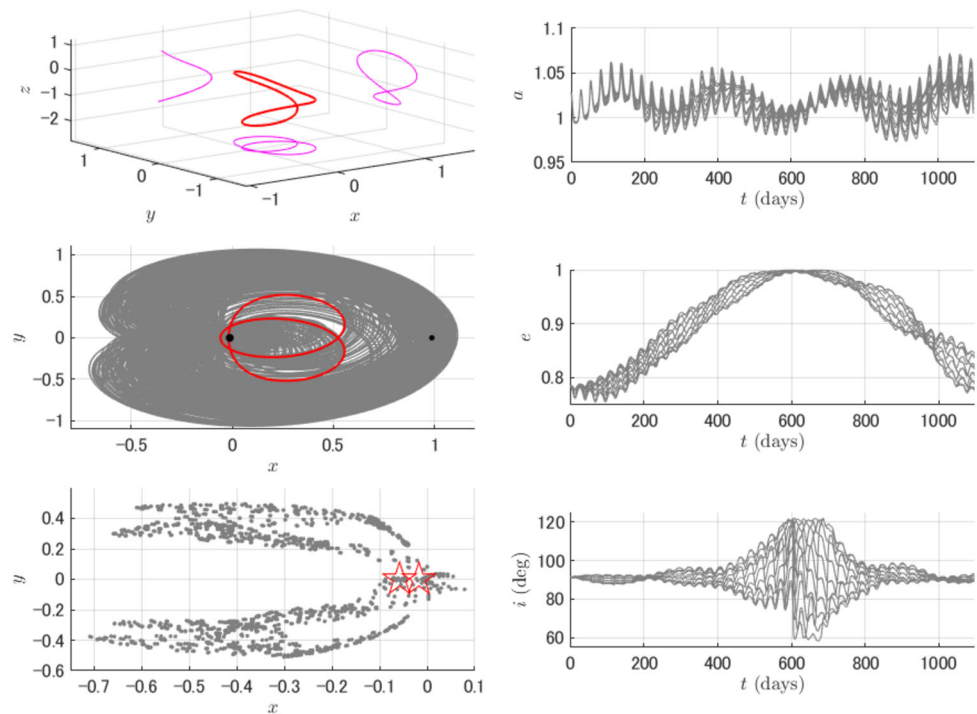


**Fig. 18** Time evolutions of the eccentricity and inclination of the unstable manifolds emanating from the periodic orbit of the sample (15) propagated in the Earth–Moon CR3BP. The difference in the colours corresponds to the different signs of the perturbation in Eq. (20) (magenta is used for  $+\epsilon$  and green is used for  $-\epsilon$ )

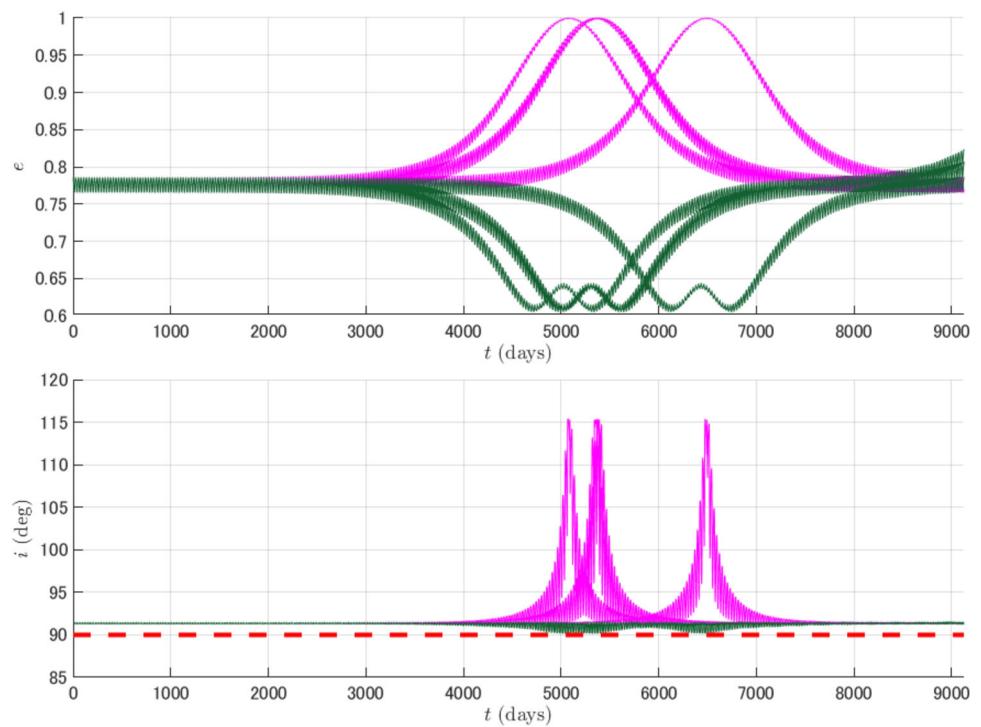


Figure 18 shows time evolutions of the eccentricity and inclination of the unstable manifolds propagated in the Earth–Moon CR3BP. The difference in the colours corresponds to the different signs of the perturbation in Eq. (20) (magenta is used for  $+\epsilon$  and green is used for  $-\epsilon$ ). The extreme behaviours reaching  $e \approx 1$  are still valid for the half

of the unstable manifolds, but their motions remain retrograde with  $i > 90^\circ$  and orbital flips do not appear in the absence of solar gravitational perturbations. Since there is only one unstable mode for the periodic orbit, the orbital flips are considered to be peculiar to the spatial BCR4BP dynamics.

## 5 Conclusion

The present paper has investigated linearly stable or weakly unstable periodic orbits in the vicinity of the 1 : 1 retrograde resonance with the Moon in the Earth–Moon spatial CR3BP. The characteristics of the periodic orbits have been analysed on a surface of section based on the geocentric orbital elements and the linear stability. We have found that many of the linearly stable periodic orbits are robust against solar gravitational perturbations, whereas some are substantially destabilised. Several weakly unstable periodic orbits of various inclinations may possess non-negligible performance of capturing objects in a sticky manner. Highly eccentric and highly inclined orbits exhibit orbital flips between prograde and retrograde states through the polar inclination, which have been suggested to be peculiar to the presence of solar gravitational perturbations.

**Acknowledgements** This study has been partially supported by JSPS Grants-in-Aid No. 20K14951.

**Data Availability** The data underlying this article will be shared on reasonable request to the corresponding author.

## Declarations

**Conflict of Interest** The author has no competing interests to declare that are relevant to the content of this article.

## References

- Bezrouk, C., Parker, J.S.: Long term evolution of distant retrograde orbits in the Earth–Moon system. *Astrophys. Space Sci.* **362**, 176 (2017)
- Boudad, K.K., Howell, K.C., Davis, D.C.: Dynamics of synodic resonant near rectilinear halo orbits in the bicircular four-body problem. *Adv. Space Res.* **66**, 2194–2294 (2020)
- Broucke, R.A.: Periodic orbits in the restricted three-body problem with Earth–Moon masses. JPL technical report 32-1168. Pasadena, Jet Propulsion Laboratory, California Institute of Technology (1968)
- Contopoulos, G., Harsoula, M.: Stickiness effects in chaos. *Celest. Mech. Dyn. Astron.* **107**, 77–92 (2010)
- Dei Tos, D.A., Russell, R.P., Topputo, F.: Survey of Mars ballistic capture trajectories using periodic orbits as generating mechanisms. *J. Guid. Control Dyn.* **41**, 1227–1242 (2018)
- Gómez, G., Jorba, À., Masdemont, J., Simó, C.: Dynamics and Mission Design Near Libration Points, Vol IV: Advanced Methods for Triangular Points. World Scientific, Singapore (2001)
- Koon, W.S., Lo, M.W., Marsden, J.E., Ross, S.D.: Dynamical Systems, the Three-Body Problem and Space Mission Design. Marsden Books, Wellington (2011)
- Kotoulas, T., Voyatzis, G.: Planar retrograde periodic orbits of the asteroids trapped in two-body mean motion resonances with Jupiter. *Planet. Space Sci.* **182**, 104846 (2020)
- Kotoulas, T., Voyatzis, G., Morais, M.H.M.: Three-dimensional retrograde periodic orbits of asteroids moving in mean motion resonances with Jupiter. *Planet. Space Sci.* **210**, 105374 (2022)
- Lara, M., Russell, R., Villac, B.F.: Classification of the distant stability regions at Europa. *J. Guid. Control Dyn.* **30**, 409–418 (2007)
- Li, M., Huang, Y., Gong, S.: Centaurs potentially in retrograde co-orbit resonance with Saturn. *Astron. Astrophys.* **617**, A114 (2018)
- Li, M., Huang, Y., Gong, S.: Survey of asteroids in retrograde mean motion resonances with planets. *Astron. Astrophys.* **630**, A60 (2019)
- Minghu, T., Ke, Z., Meibo, L., Chao, X.: Transfer to long term distant retrograde orbits around the Moon. *Acta Astronaut.* **98**, 50–63 (2014)
- Morais, M.H.M., Namouni, F.: Retrograde resonance in the planar three-body problem. *Celest. Mech. Dyn. Astron.* **117**, 405–421 (2013)
- Morais, M.H.M., Namouni, F.: A numerical investigation of coorbital stability and libration in three dimensions. *Celest. Mech. Dyn. Astron.* **125**, 91–106 (2016)
- Morais, M.H.M., Namouni, F.: Periodic orbits of the retrograde coorbital problem. *Mon. Not. R. Astron. Soc.* **490**, 3799–3805 (2019)
- Morais, M.H.M., Namouni, F., Voyatzis, G., Kotoulas, T.: A study of the 1/2 retrograde resonance: periodic orbits and resonant capture. *Celest. Mech. Dyn. Astron.* **133**, 21 (2021)
- Oshima, K.: Retrograde co-orbital orbits in the Earth–Moon system: planar stability region under solar gravitational perturbation. *Astrophys. Space Sci.* **366**, 88 (2021)
- Oshima, K., Yanao, T.: Spatial unstable periodic quasi-satellite orbits and their applications to spacecraft trajectories. *Celest. Mech. Dyn. Astron.* **131**, 23 (2019)
- Russell, R.P.: Global search for planar and three-dimensional periodic orbits near Europa. *J. Astronaut. Sci.* **54**, 199–226 (2006)
- Simó, C., Gómez, G., Jorba, À., Masdemont, J.: The bicircular model near the triangular libration points of the RTBP. In: Roy, A.E., Steves, B.A. (eds.) *From Newton to Chaos*. Springer, Boston (1995)
- Slíz-Balogh, J., Barta, A., Horváth, G.: Celestial mechanics and polarization optics of the Kordylewski dust cloud in the Earth–Moon Lagrange point L5-I. Three-dimensional celestial mechanical modelling of dust cloud formation. *Mon. Not. R. Astron. Soc.* **480**, 5550–5559 (2018)
- Slíz-Balogh, J., Barta, A., Horváth, G.: Celestial mechanics and polarization optics of the Kordylewski dust cloud in the Earth–Moon Lagrange point L5-II. Imaging polarimetric observation: new evidence for the existence of Kordylewski dust cloud. *Mon. Not. R. Astron. Soc.* **482**, 762–770 (2019)
- Szebehely, V.: *Theory of Orbits: The Restricted Problem of Three Bodies*. Academic Press Inc., New York (1967)
- Topputo, F.: On optimal two-impulse Earth–Moon transfers in a four-body model. *Celest. Mech. Dyn. Astron.* **117**, 279–313 (2013)
- Wiegert, P., Connors, M., Veillet, C.: A retrograde co-orbital asteroid of Jupiter. *Nature* **543**, 687–689 (2017)

**Publisher's Note** Springer Nature remains neutral with regard to jurisdictional claims in published maps and institutional affiliations.